

## Popular Summary for

The relationship of loss, mean age of air and the distribution of CFCs to stratospheric circulation and implications for atmospheric lifetimes

A. R. Douglass<sup>1</sup>, R. S. Stolarski<sup>1</sup>, M. R. Schoeberl<sup>1</sup>, C. H. Jackman<sup>1</sup>, M. L. Gupta<sup>1,4</sup>,  
P. A. Newman<sup>1</sup>, J. E. Nielsen<sup>2,3</sup>, E. L. Fleming<sup>3</sup>

submitted to Journal of Geophysical Research, November 2007

Man-made molecules called chlorofluorocarbons (CFCs) are broken apart in the stratosphere by high energy light, and the reactive chlorine gases that come from them cause the ozone hole. Since the ozone layer stops high energy light from reaching low altitudes, CFCs must be transported to high altitudes to be broken apart. The number of molecules per volume (the density) is much smaller at high altitudes than near the surface, and CFC molecules have a very small chance of reaching that altitude in any particular year. Many tons of CFCs were put into the atmosphere during the end of the last century, and it will take many years for all of them to be destroyed. Each CFC has an atmospheric lifetime that depends on the amount of energy required to break them apart. Two of the gases that were made the most are  $\text{CFCl}_3$  and  $\text{CF}_2\text{Cl}_2$ . It takes more energy to break apart  $\text{CF}_2\text{Cl}_2$  than  $\text{CFCl}_3$ , and its lifetime is about 100 years, nearly twice as long as the lifetime for  $\text{CFCl}_3$ . It is hard to figure out the lifetimes from surface measurements because we don't know exactly how much was released into the air each year.

Atmospheric models are used to predict what will happen to ozone and other gases as the CFCs decrease and other gases like  $\text{CO}_2$  continue to increase during the next century. CFC lifetimes are used to predict future concentrations and all assessment models use the predicted future concentrations. The models have different circulations and the amount of CFC lost according to the model may not match the loss that is expected according to the lifetime. In models the amount destroyed per year depends on how fast the model pushes air into the stratosphere and how much goes to high altitudes each year. This paper looks at the way the model circulation changes the lifetimes, and looks at measurements that tell us which model is more realistic. Some models do a good job reproducing the age-of-air, which tells us that these models are circulating the stratospheric air at the right speed. These same models also do a good job reproducing the amount of CFCs in the lower atmosphere where they were measured by instruments on NASA's ER-2, a research plane that flies in the lower stratosphere. The lifetime for  $\text{CFCl}_3$  that is calculated using the models that do the best job matching the data is about 25% longer than most people thought. This paper shows that using these measurements to decide which models are more realistic helps us understand why their predictions are different from each other and also to decide which predictions are more likely.

<sup>1</sup>Atmospheric Chemistry and Dynamics Branch, Code 613.3, NASA Goddard Space Flight Center, Greenbelt, Maryland, USA

<sup>2</sup>Global Modeling and Assimilation Office, Code 610.1, NASA Goddard Space Flight Center, Greenbelt, Maryland, USA

<sup>3</sup>Science Systems and Applications, Inc., Lanham, Maryland, USA

<sup>4</sup>Present Affiliation, Federal Aviation Administration, Washington, DC, USA

The relationship of loss, mean age of air and the distribution of CFCs to stratospheric  
circulation and implications for atmospheric lifetimes

A. R. Douglass<sup>1</sup>, R. S. Stolarski<sup>1</sup>, M. R. Schoeberl<sup>1</sup>, C. H. Jackman<sup>1</sup>, M. L. Gupta<sup>1,4</sup>,  
P. A. Newman<sup>1</sup>, J. E. Nielsen<sup>2,3</sup>, E. L. Fleming<sup>3</sup>

November 5, 2007

<sup>1</sup>Atmospheric Chemistry and Dynamics Branch, Code 613.3, NASA Goddard Space  
Flight Center, Greenbelt, Maryland, USA

<sup>2</sup>Global Modeling and Assimilation Office, Code 610.1, NASA Goddard Space Flight  
Center, Greenbelt, Maryland, USA

<sup>3</sup>Science Systems and Applications, Inc., Lanham, Maryland, USA

<sup>4</sup>Present Affiliation, Federal Aviation Administration, Washington, DC, USA

1   **Abstract**

2   Projections of the recovery of the ozone layer are made with global atmospheric models  
3   using a specified time-series of mixing ratios of ozone depleting substances (ODSs) at the  
4   lower boundary. This time-series is calculated using observations, emission rates, and an  
5   estimate for the atmospheric lifetime. ODS destruction and simulated atmospheric-  
6   lifetime vary among models because they depend on the simulated stratospheric transport  
7   and mixing. We investigate the balance between the annual change in ODS burden, its  
8   atmospheric loss, and the annual ODS input to the atmosphere using several models.  
9   Some models reproduce realistic distributions for the mean age of air and some do not.  
10   Models with faster circulations produce 'young' distributions for the age of air and fail to  
11   reproduce the observed relationship between the mean age of air at a particular location  
12   and the amount of ODS at that location relative to its initial value (i.e., the fractional  
13   release). Models with realistic mean age of air reproduce this observed relationship.  
14   These models yield a lifetime for  $\text{CFCl}_3$  of ~56 years, longer than the 45 year lifetime  
15   used to project future mixing ratios. The residual circulation of our chemistry climate  
16   model speeds up as climate changes. The lifetime of  $\text{CFCl}_3$  decreases to ~52 years by  
17   2050 due to the circulation change. Use of flux boundary conditions in assessment  
18   models rather than specified mixing ratios would produce simulations in which ODS  
19   evolution is consistent with simulated loss, including the time dependence of the loss due  
20   to circulation change.

21

22

22 **1. Introduction**

23 Current ozone assessment efforts have two main goals. The first is to verify that the  
24 ozone decreases of the 1980's and 1990's have ceased. The second is to predict the  
25 behavior of the ozone layer, as the atmospheric burden of green house gases increases  
26 and the concentrations of chlorofluorocarbons (CFCs) decline. The CFC decline is due to  
27 cessation of production and continued atmospheric loss mainly through photolysis by  
28 ultraviolet radiation in the stratosphere (e.g., Chapter 8 of *Scientific Assessment of Ozone*  
29 *Depletion: 2006* [WMO, 2007, hereafter referred to as WMO2007]). This paper is  
30 focused on the second goal, and examines the consistency between the annual change in  
31 the integrated atmospheric amount, the computed atmospheric loss and the input of CFCs  
32 to the atmosphere implied by the boundary conditions.

33

34 The procedures used to produce the timeseries of CFC mixing ratios that are used in  
35 assessments are discussed in detail in Chapter 8 of WMO2007. These boundary  
36 conditions, specified at the lowest model layer, largely control the time evolution of the  
37 atmospheric burden of the source gases (i.e., the total mass of the source gas in the  
38 atmosphere) in all assessment models because the variations of the mass of source gases  
39 in the stratosphere among the models are small compared with the mass of the source gas  
40 in the troposphere. Projections for the recovery of the ozone hole using semi-empirical  
41 models also rely on these predicted mixing ratios for chlorine and bromine source gases  
42 [e.g., *Newman et al.*, 2006].

43

44 Mixing ratio boundary conditions have been used in assessments since the late 1980s.  
45 Prior assessments pre-dated international agreements to control CFC production, and  
46 used a combination of emissions and mixing ratios to focus on the ozone change in the  
47 upper atmosphere (e.g., *Atmospheric Ozone 1985: Assessment of our Understanding of*  
48 *the Processes Controlling its present Distribution and Change*, [WMO 1985]). In  
49 contemporary assessment calculations the mixing ratio boundary conditions largely  
50 control the evolution of the mixing ratios of  $\text{Cl}_y$  and its components in the upper  
51 stratosphere where nearly all the CFCs have been destroyed. The time evolution of  $\text{Cl}_y$   
52 depends slightly on the circulation. For example, a more rapid overturning stratospheric  
53 circulation will produce a peak in  $\text{Cl}_y$  a year or two ahead of a slower circulation.

54  
55 The dependence on the circulation is apparent in the distributions of CFCs and  $\text{Cl}_y$  in the  
56 lower stratosphere. *Waugh et al.* [2007] use CTM simulations using different  
57 meteorological fields, horizontal resolution and upper boundary height to show how  
58 differences in simulated transport and mixing affect the net destruction of the source  
59 gases and the distributions of  $\text{Cl}_y$ . The models shown in Figure 6.8 of WMO2007 use the  
60 same boundary conditions, yet the peak October zonal mean inorganic chlorine ( $\text{Cl}_y$ ) at  
61 50 hPa 80°S exhibits a spread of about 0.75 ppbv (~25%) ignoring outliers.

62  
63 Despite the difference in the peak amounts of  $\text{Cl}_y$ , its evolution over time is similar  
64 among most of the models. In the WMO2007 models  $\text{Cl}_y$  increases substantially between  
65 1980 and 2000, and decreases by a similar amount between 2005 and about 2050 in direct  
66 response to the imposed mixing ratio boundary conditions. Here we show that the

67 constraint on the overall evolution of the CFCs and  $Cl_y$  produces inconsistency between  
68 the annual change in burden (prescribed by the boundary conditions) and the simulated  
69 loss.

70

71 In addition to their use in predicting the future mixing ratios of CFCs, atmospheric  
72 lifetimes are important to the evaluation of the reservoirs of CFCs called banks. Banks  
73 exist because CFCs have commonly been used in closed applications such as  
74 refrigeration and air conditioning. As long as the appliances remain operational, the  
75 CFCs are sealed and not released to the atmosphere. The magnitude and rate of release  
76 of CFCs from these banks are subjects of debate. A 'top down' estimate of a bank is the  
77 cumulative difference of estimated production and the emission inferred from  
78 atmospheric observations using a model and a presumed lifetime. A 'bottom-up' bank  
79 estimates rely on a detailed analysis of applications that sequester the CFCs [McCullough  
80 *et al.*, 2001; McCullough *et al.*, 2003]. The top-down analysis was used by *Scientific*  
81 *Assessment of Ozone Depletion: 1998* [WMO, 1999] and *Scientific Assessment of Ozone*  
82 *Depletion: 2002* [WMO, 2003]. The bottom-up analysis is used by *Special Report:*  
83 *Safeguarding the ozone layer and the global climate system: Issues related to*  
84 *hydrofluorocarbons and perfluorocarbons* [IPCC, 2005]. Daniel *et al.* [2007] analyze the  
85 banks computed from a 'top down' analysis versus those computed from a bottom-up  
86 analysis. The maximum annual global emissions of chlorofluorocarbons (CFCs) took  
87 place during the late 1980s prior to the international agreements to ban production (~ 350  
88 Ktons/year for  $CFCl_3$  and ~ 460 Ktons/year for  $CF_2Cl_2$ ). These are far greater than  
89 estimates of emissions from banks, but the emissions from the banks are presently

90 comparable to annual atmospheric loss estimates and differences in the bank estimates  
91 are significant for decadal predictions. *Daniel et al. op cit.* point out that even small  
92 errors in lifetime accumulate, leading to uncertainty in the top-down bank estimates and  
93 also show that differences in bank estimates are large enough to impact predictions for  
94 future levels of CFCs and ozone recovery.

95

96 The purpose of this paper is to use a variety of model simulations to investigate the  
97 relationships among the atmospheric burden, the lifetime and the loss rates of CFCs. We  
98 present results from simulations that have both realistic and unrealistic distributions for  
99 the stratospheric age-of-air. We show that the lower stratospheric relationships between  
100 the fractional release of chlorine from  $\text{CFCl}_3$  and  $\text{CF}_2\text{Cl}_2$  and the age-of-air produced by  
101 simulations with realistic age-of-air match relationships derived from aircraft  
102 observations by *Schauffler et al.* [2003]. Models with faster circulations do not produce  
103 realistic age-of-air and also do not reproduce the observed relationship between fractional  
104 release and mean age. In all simulations the annual change in atmospheric burden is  
105 specified by the mixing ratio boundary conditions and is thus disconnected from the  
106 simulation loss. The fluxes are free to obtain any value as determined by interior  
107 transport and loss rates. In simulations with 'young' age-of-air the CFC lifetime is equal  
108 to or shorter than that presumed in WMO2007 and the inferred boundary flux of CFCs  
109 can be unrealistically large in the early part of the present century. In simulations with  
110 realistic age-of-air, the lifetime is longer than presumed in WMO2007 and the inferred  
111 boundary flux of CFCs is negative after about 2010. The negative flux is computed

112 because the annual decrease in atmospheric burden imposed by the boundary conditions  
113 exceeds the simulated loss.

114

115 The models used in this analysis are described in the following section. Simulation  
116 results are presented in section 3. In section 4 we build on the results of *Hall* [2000] and  
117 *Schoeberl et al.* [2000], using trajectory simulations of age spectra and annual  
118 stratospheric loss rates to explain the relationship between the mean age-of-air and the  
119 fractional release of CFCs. The implications of the comparisons with observations for  
120 determination of CFC lifetime and removal from the atmosphere are discussed in section  
121 5. We also consider the possibility that a speed-up in the Brewer Dobson Circulation due  
122 to climate change will impact the annual CFC loss and thus the ozone recovery [e.g.,  
123 *Butchart and Scaife*, 2001]. Conclusions follow in section 6.

124

## 125 **2. Model Descriptions**

126 Two types of atmospheric numerical models are used to predict the response of ozone to  
127 changes in the composition and climate of the atmosphere. A chemistry/climate model  
128 (CCM) combines a representation of photochemical processes with a general circulation  
129 model (GCM). In a CCM, ozone and other radiatively active gases are transported by the  
130 simulation winds, and the computed constituent fields are used to compute net radiative  
131 heating rates for the GCM, ensuring consistency among dynamics, radiation and  
132 photochemistry. A chemistry transport model (CTM) differs from a CCM in that the  
133 meteorological information needed for constituent transport and to account for  
134 temperature dependence of photochemical processes is input to the model from an

135 external source such as a GCM or a data assimilation system. CTMs may be three-  
136 dimensional or two-dimensional (latitude/altitude) but heating rates that would be  
137 calculated from trace gas distributions in CTMs are not necessarily consistent with the  
138 input meteorological fields.

139

140 The surface boundary conditions for source gases including chlorofluorocarbons are  
141 specified for all simulations following scenario A1B of the *Scientific Assessment of*  
142 *Ozone Depletion: 2002* [WMO, 2002]. Scenario A1B was also used in the modeling  
143 studies presented in WMO2007. Another scenario, A1, presented in Table 8-5 of  
144 WMO2007 is virtually the same as scenario A1B up to 2010. Although there differences  
145 between scenarios A1B and A1 after 2010, these will not impact the results of this study.  
146 The models used for these multi-decadal simulations are described below; the simulations  
147 are summarized in Table 1.

148

149 We also use a trajectory approach described by *Schoeberl et al.* [2000] to produce age  
150 spectra and to interpret the relationship between the mean age of air and the constituent  
151 distributions. The trajectory model is summarized after descriptions of the CCM and the  
152 CTMs.

153

154 *The GEOS-4 CCM*

155 The Goddard CCM, described briefly by *Stolarski et al.* [2006a], combines the GEOS-4  
156 GCM (Goddard Earth Observing System, Version 4, General Circulation Model) with a  
157 representation of stratospheric photochemistry. Here we refer to this model as CGCM.

158 *Pawson et al.* [2007] describe CGCM and its performance. The GCM dynamical core  
159 uses a flux form semi-Lagrangian transport scheme [*Lin and Rood*, 1996, 1997] and a  
160 quasi-Lagrangian vertical coordinate system [*Lin*, 1997] to ensure accurate representation  
161 of the transport by the resolved-scale flow. The *Lin and Rood* [1996] transport scheme is  
162 also used for constituent advection. The photochemical mechanism includes all  
163 photolytic, gas-phase and heterogeneous reactions thought to be of importance in the  
164 stratosphere. The photochemical scheme, an updated version of that used in the Goddard  
165 CTM [e.g., *Dougllass and Kawa*, 1999 and references therein] uses family  
166 approximations and has been extensively tested through applications of the Goddard  
167 CTM [*Dougllass et al.*, 2001; *Stolarski et al.* 2006b]. Reaction rate and cross section data  
168 are taken from the Jet Propulsion Laboratory Evaluation 14 [*Sander et al.*, 2003].  
169 Processes involving polar stratospheric clouds use the parameterization described by  
170 *Considine et al.* [2000]. In the troposphere ozone relaxes to the climatology described by  
171 *Logan* [1999]. The ozone simulated using the CTM with meteorological fields from the  
172 GCM was shown to compare well with the ozone climatology used in the GCM before  
173 attempting to couple the GCM and photochemistry. A clock tracer is included in the  
174 simulation, providing information about the three-dimensional distribution of the mean  
175 age of air but no information about the age spectrum. The spatial resolution for  
176 simulations presented here is 2° latitude by 2.5° longitude with 55 layers from the surface  
177 to 0.01 hPa. The Brewer Dobson circulation is shown to be realistic by comparisons with  
178 observations showing the rate of ascent of tropical moisture anomalies and the decrease  
179 of the amplitude of the anomalies with height [*Eyring et al.*, 2006]. A weakness of the  
180 CGCM, common among CCMs, is that its south polar vortex lasts several weeks longer

181 than is consistent with observations [Eyring *et al.*, 2006; Pawson *et al.*, 2007]. This  
182 deficiency will have minimal impact on the computed CFC lifetime. The CGCM  
183 simulations used in this work differ in duration, and source of sea surface temperatures  
184 (SST) and sea-ice distributions at the lower boundary. Past simulations (1950 – 2004 use  
185 the “HadISST” (Hadley Center Ice and Sea-Surface Temperature) data set of Rayner *et*  
186 *al.* [2003]. Future simulations are integrated until 2049 or later, and use output from  
187 coupled ocean-atmosphere model simulations: HadGem1 [Johns *et al.*, 2006] and NCAR  
188 CCSM3 [Kiehl *et al.*, 1998]. The CGCM simulations are summarized in Table 1. The  
189 CGCM simulations using the various SSTs are similar but not identical. Results shown  
190 below are from specific simulations, but the same conclusions are drawn from any of the  
191 simulations.

192

### 193 *Global Modeling Initiative CTM*

194 Strahan and Douglass [2004] and Douglass *et al.* [2004] describe and evaluate the GMI  
195 CTM and the simulations used here. This version of the GMI CTM uses the same  
196 advection scheme, the same look-up tables for the photolysis calculation and essentially  
197 the same photochemical mechanism as the CGCM described above. Horizontal  
198 resolution for these simulations is 4° latitude x 5° longitude, with 28 vertical levels from  
199 the surface to 0.4 hPa. Individual species are advected separately with the exception of  
200 some radical species, and the photochemical contribution to the individual tendency  
201 equations are calculated using SMVGear II [Jacobson, 1998]. Experiments in which a  
202 ‘pulse’ of a conserved tracer is emitted and tracked provide information about the annual  
203 mean age of air and the age spectrum. The two simulations differ only in the input  
204 meteorological fields. One set of meteorological fields is taken from a GCM that uses a

205 version of the GEOS-4 GCM dynamical core described above and was developed  
206 through a collaboration of NASA with the National Center for Atmospheric Research.  
207 The second set of fields is taken from a version of the Goddard Earth Observing System  
208 Data Assimilation System (GEOS-DAS). This version of GEOS-DAS uses this same  
209 GCM in the assimilation process. *Strahan and Douglass* [2004] and *Douglass et al.*  
210 [2004] provide many details about the input meteorological fields and extensive  
211 comparisons with observations. The comparisons show that the short-lived radicals such  
212 as ClO and NO<sub>2</sub> and longer-lived reservoir species such as HCl, ClONO<sub>2</sub> and HNO<sub>3</sub>  
213 compare well with observations. However, the overturning circulation associated with  
214 this version of GEOS-DAS is much more rapid than that produced by the GCM, and  
215 comparisons involving long-lived source gases show that transport produced by the GCM  
216 fields is more realistic than that produced using the assimilated meteorology [*Douglass et*  
217 *al.*, 2003]. In the remainder of this paper, simulations using the GMI CTM with  
218 meteorological fields from the GCM and GEOS-DAS are referred to as GMI-GCM and  
219 GMI-DAS respectively.

220

### 221 *Two-Dimensional CTM*

222 The GSFC two-dimensional (2D) CTM, originally discussed in *Douglass et al.* [1989]  
223 and *Jackman et al.* [1990], has undergone steady upgrades and improvements [*Fleming et*  
224 *al.*, 2007 and references therein]. The present version uses changing transport fields over  
225 the 1958-2004 period and a climatology for years 2005-2050, all from the National  
226 Centers for Environmental Prediction- National Center for Atmospheric Research  
227 reanalysis project. *Fleming et al.* [2007] show that long-lived tracers produced using

228 these transport fields compare well with observations. Here the 2D CTM vertical domain  
 229 extends from the ground to approximately 92 km with levels separated by ~2 km. The  
 230 horizontal domain extends from pole to pole, with 18 boxes of 10 degrees latitude. The  
 231 photochemical mechanism includes largely the same reactions as used in the 3D models  
 232 described above, and also uses kinetic information from the Jet Propulsion Laboratory  
 233 Evaluation 14 [*Sander et al.*, 2003]. Simulations using this most recent updated version  
 234 of the 2D CTM are referred to here as 2D-base.

235

236 An earlier version of the 2D CTM, the "1995 model" described in *Fleming et al.* [1999,  
 237 2001] produces much shorter age-of-air than indicated by measurements. This version of  
 238 the 2D CTM is referred to as 2D-fast and provides a contrast to the more realistic 2D-  
 239 base version.

240

241 Table 1: A summary of the simulations used in this work. SST1= observed (Hadley);  
 242 SST2= Modeled HadGEM1; SST3=Modeled NCAR CCM3

model	duration	Realistic Age of air
2D-base	1935 - 2099	yes
2D-fast	1935 - 2099	no
GMI-GCM	1995 - 2030	yes
GMI-DAS	1995 - 2030	no
CGCM		
P1 SST1	1950 - 2004	yes
P2 SST1	1950 - 2004	yes

F1 SST2	1996 – 2099	yes
F2 SST2	1971 – 2049	yes
F3 SST3	1971 – 2052	yes
F4 SST3	2000 – 2099	yes

243

244 *Trajectory Model*

245 *Schoeberl et al.* [2000, hereafter S2000] describe the 2D trajectory model in detail. The  
 246 trajectory model uses the residual circulation and mixing coefficients of the 2D CTM.  
 247 The residual circulation is computed from diabatic heating rates, and the trajectory model  
 248 scrambles vertical and horizontal positions to simulate mixing [*Feller, 1968*]. S2000  
 249 show that the parcel spectra produced by long simulations using a 3D trajectory model  
 250 are similar to those produced by this 2D model. The 2D trajectory model is used because  
 251 it is more than 100 times faster than an equivalent 3D calculation.

252

253 **3. Simulation Results**

254 Simulated fields for the present and near past can be compared with data from various  
 255 sources to evaluate the representation of the atmosphere by the model. Here we make  
 256 some comparisons with observations in order to assess the potential uncertainties in any  
 257 projections into the future and contrast results from different simulations.

258

259 *Loss Rate Distributions*

260 The annual average local lifetimes (inverse of the local chemical loss frequency) for  
 261  $\text{CFCl}_3$  and  $\text{CF}_2\text{Cl}_2$  are shown in Figure 1. The shading emphasizes the narrow transition

262 separating a region with a lifetime of two years or longer from a region with lifetimes of  
263 a few months or less. For  $\text{CFCl}_3$  ( $\text{CF}_2\text{Cl}_2$ ) parcels below 50 hPa (20 hPa) outside the  
264 tropics have local lifetimes of two years or longer. Air parcels that remain below the  
265 shaded transition region retain most of their  $\text{CFCl}_3$  ( $\text{CF}_2\text{Cl}_2$ ) while those that go above the  
266 transition have their  $\text{CFCl}_3$  ( $\text{CF}_2\text{Cl}_2$ ) rapidly converted to  $\text{Cl}_y$ .

267

268 We compare results from the five simulations with the models described in Section 2 to  
269 demonstrate the relationship of the circulation to the loss rates and time-evolving burden  
270 of chlorofluorocarbons. The annual-averaged loss distributions ( $\# \text{ cm}^{-3} \text{ s}^{-1}$ ) for each of the  
271 simulations are shown for  $\text{CFCl}_3$  and  $\text{CF}_2\text{Cl}_2$  for the year 2000 in Figure 2. For  $\text{CFCl}_3$   
272 most of the loss takes place in the tropics below 10 hPa. There is no significant loss  
273 above 10 hPa because destruction below is sufficiently rapid that  $\text{CFCl}_3$  is destroyed  
274 before parcels reach that level. Parcels between 10 and 30 hPa at middle latitudes are  
275 similarly depleted of  $\text{CFCl}_3$  so there is little loss in spite of short chemical lifetimes.  
276 Parcels in the lower stratosphere middle latitudes contribute little to the loss because the  
277 destruction rate is slow. A similar discussion applies to the loss distributions for  $\text{CF}_2\text{Cl}_2$ ,  
278 but the region of the greatest loss is found at a higher altitude as expected from the  
279 difference in lifetimes (Figure 1).

280

281 It is clear from Figure 2 that the simulations with faster circulations (GMI-DAS and 2D-  
282 fast) have larger total loss rates than the CGCM, GMI-GCM and 2D-base. Stronger  
283 upwelling shifts the tropical constituent profiles upward and the loss, the product of the  
284 mixing ratio and the destruction rate, is commensurately greater.

285 *Age of Air and Cl<sub>y</sub> Distributions*

286 Circulation differences among the models are also apparent through comparison of the  
287 stratospheric age-of-air derived from the simulations. These differences can be evaluated  
288 by comparison to observations [Boering *et al.*, 1996] as in Figure 3. The values produced  
289 by the CGCM, 2D-base and GMI-GCM fall within the  $2\sigma$  limits of values derived from  
290 observations poleward of about  $15^\circ$  latitude. There is a small offset in the tropics. The  
291 2D-fast and GMI-DAS simulations both produce age distributions that are young  
292 compared with the values derived from observations, and could both be described as  
293 having fast circulations. The other three could be said to have realistic (slow)  
294 circulations.

295

296 An important test of the circulation and its interaction with photochemical destruction is  
297 provided by the fractional release of chlorine from CFCs. In the upper stratosphere,  
298  $\text{CFCl}_3$  and  $\text{CF}_2\text{Cl}_2$  are nearly completely photolyzed in all simulations, and  $\text{Cl}_y$  time  
299 series from different simulations are nearly identical, as shown by time series for GMI-  
300 GCM and GMI-DAS at  $2^\circ\text{N}$  and 1.3 hPa in Figure 4(a). The  $\text{Cl}_y$  distributions are quite  
301 different in the two simulations below 10 hPa with significantly higher values of  $\text{Cl}_y$  in  
302 GMI-GCM compared with GMI-DAS as shown for annually averaged  $\text{Cl}_y$  in Figure 4(b).  
303 The differences are greater than 10 percent for most of the region between 70 and 10 hPa,  
304 and are greater than 30% in much of the southern hemisphere (Figure 4(c)). We test the  
305 realism of the 'fast' versus the 'slow' circulation using aircraft observations of  $\text{CFCl}_3$  and  
306  $\text{CF}_2\text{Cl}_2$

307

308 *Fractional Release*

309 *Schauffler et al.* [2003] use aircraft observations of various long-lived source gases to  
310 compute the fractional release (fr)

$$311 \quad \text{fr} = (1 - \chi(\mathbf{x})/\chi_i)$$

312 where  $\chi(\mathbf{x})$  is the mixing ratio of a chlorofluorocarbon in a parcel at location  $\mathbf{x}$  (latitude,  
313 altitude, pressure, time) and  $\chi_i$  is the mixing ratio that the parcel would have had no loss  
314 occurred. We estimate  $\chi_i$  using the mean age to determine the constituent mixing ratio at  
315 the time of entry at the tropical tropopause (i.e., the time of the measurement of  $\chi$  minus  
316 the mean age). We tested this approximation by comparing the mean of the distribution  
317 of initial mixing ratios calculated from the constituent time series at the tropical  
318 tropopause using the GMI age spectra calculated with  $\chi_i$  calculated using the mean age.  
319 The age spectra are not symmetric and have a tail of elements corresponding to older ages.  
320 Each element  $j$  is associated with a different entry value  $\chi_i^j$  because the CFCs are  
321 increasing with time. The means of the initial values associated with each element in the  
322 age spectrum are only a few percent smaller than values  $\chi_i$  calculated using the mean age.

323

324 *Schauffler et al.* [2003] find a compact relationship between mean age of air and the  
325 fractional release in the lower stratosphere using observations from several aircraft  
326 campaigns. The simulations considered here produce compact relationships for  $\text{CFCl}_3$   
327 and  $\text{CF}_2\text{Cl}_2$  at  $\sim 50$  hPa (a comparable height to the observations). These are shown in  
328 Figure 5 along with the fractional releases and mean ages derived from observations by

329 *Schauffler et al.* [2003]. For observations and for all simulations, fractional release  
330 increases monotonically with age. Simulations using the slower circulations (CGCM,  
331 GMI-GCM and 2D-Base), with realistic values for mean age-of air (Figure 3), produce  
332 relationships between mean age and fractional release similar to those derived from  
333 observations. The fractional releases of both compounds are somewhat larger than  
334 observed for air masses with older mean age, with larger differences for  $\text{CF}_2\text{Cl}_2$ . The fast  
335 circulations (GMI-DAS and 2D-fast) produce relationships that are clearly separated  
336 from those derived from observations or produced by the other simulations (Figure 5).

337

338 The ranges of values are somewhat smaller for the GMI simulations than for any of the  
339 other simulations. The annual zonal mean age is determined for both GMI simulations  
340 using "pulse" experiments; this is plotted vs. the fractional release calculated from annual  
341 zonal mean tracer fields. The mean age for CGCM is calculated using a "clock" tracer, and  
342 its seasonal and longitudinal variations are matched with similar variations in tracer fields.  
343 The ranges of age and fractional release using annually zonal averaged fields are reduced  
344 by the temporal and spatial averaging but the relationship between them is similar to that  
345 obtained with the other simulations.

346 *Budgets for  $\text{CFCl}_3$  and  $\text{CF}_2\text{Cl}_2$*

347 The rate of change of a particular CFC's burden  $B$  satisfies a conservation equation

348 
$$\partial B/\partial t = F - B/\tau \quad (1)$$

349 where  $F$  is the flux (i.e., the emissions into the atmosphere) and  $\tau$  is the atmospheric  
350 lifetime of that CFC. In all of our simulations, the CFC mixing ratio in the boundary layer

351 is specified. Because the mass of the stratosphere is small and the entire troposphere  
 352 responds to the boundary conditions, the total atmospheric burdens of  $\text{CFCl}_3$  or  $\text{CF}_2\text{Cl}_2$   
 353 and the year-to-year changes in the atmospheric burden are largely governed by the  
 354 boundary conditions. The annual-average atmospheric losses ( $B/\tau$ ) for  $\text{CFCl}_3$  and  $\text{CF}_2\text{Cl}_2$   
 355 as functions of time for the recent past and the future are compared in Figure 6 for each  
 356 of the five simulations. Between 2000 and 2030 the integrated loss is much higher for the  
 357 two simulations with fast circulations. The simulations with different losses maintain  
 358 balance between the annual change in burden ( $\partial B/\partial t$ ), the annual loss terms  $B/\tau$  and the  
 359 input to the atmosphere with different implied fluxes of  $\text{CFCl}_3$  and  $\text{CF}_2\text{Cl}_2$  at the lower  
 360 boundary. Equation 1 can be solved for the flux necessary to produce the change in  
 361 burden that is imposed by the mixing ratio boundary conditions. The net atmospheric  
 362 losses up until 2002 for  $\text{CF}_2\text{Cl}_2$  and  $\text{CFCl}_3$  from CGCM, 2D-base and 2D-fast (the three  
 363 simulations that span the appropriate temporal domain) are compared in Table 2. The  
 364 differences among the simulations are not large compared with the estimated total input to  
 365 the atmosphere as shown by the last column which is the maximum difference divided by  
 366 the estimated total atmospheric input.

367

368 Table 2. Net atmospheric losses up until 2002 (in kilotons).

	CGCM	2D-base	2D-fast	$\Delta\text{loss}/(\text{total input})$
$\text{CFCl}_3$	2310	2630	3200	0.10
$\text{CF}_2\text{Cl}_2$	2340	2480	2730	0.03

369

370 The fluxes inferred from the burden change and simulation losses for the 2D-base and 2D-  
371 fast simulations are compared with industrial estimates in Figure 7a for  $\text{CFCl}_3$  and Figure  
372 7b for  $\text{CF}_2\text{Cl}_2$ . Fluxes were not shown for the GMI simulations as they begin in 1995  
373 when emissions to the atmosphere have already declined substantially from their late  
374 1980's maxima. The CGCM simulations are not shown because they used the mixing  
375 ratios recorded on the CCMVal website at 5-year intervals with a linear interpolation  
376 between. This does not alter any of the results presented here, but the deduced flux has  
377 unrealistic jumps at 5- year intervals.

378

379 Up until about 1980 the emissions of CFCs increase rapidly and the change in burden  
380 ( $\partial B/\partial t$ ) is significantly larger than the photochemical loss for a given year ( $\partial B/\partial t \gg B/\tau$ ,  
381 so  $\partial B/\partial t \approx F$ ), thus differences in the simulated loss rates lead to very small differences in  
382 the deduced flux. In later years, as  $\partial B/\partial t$  decreases, the model differences in the total loss  
383 rates leads to a substantial difference in the fluxes deduced for the fast and realistic  
384 simulations. The  $\text{CFCl}_3$  flux computed with 2D base is consistently smaller than the  
385 bottom-up estimate of emissions [McCullough *et al.*, 2001]. The 2D base  $\text{CF}_2\text{Cl}_2$  flux is  
386 also smaller than the bottom-up estimate [McCullough *et al.*, 2003], but the discrepancy  
387 is smaller. We infer from differences in the losses in Figure 6 that the CGCM flux for  
388  $\text{CF}_2\text{Cl}_2$  would be closer to the data while that for  $\text{CFCl}_3$  would be in worse agreement.  
389 This inconsistency for  $\text{CFCl}_3$  but not for  $\text{CF}_2\text{Cl}_2$  is similar to results obtained by Gupta *et*  
390 *al.* [2001], who compare computed surface mixing ratios with observations and conclude

391 that the  $\text{CFCl}_3$  emissions are too large. The CFC lifetimes produced by the model used  
392 by *Gupta et al.* [2001] are similar to those produced by the CGCM.  
393  
394 The differences in the losses are also significant in the later years, after ~2020, when the  
395 input of CFCs to the atmosphere is expected to be negligible (i.e.,  $F \approx 0$ ). We compare the  
396 fluxes inferred from the burden change and the simulated losses for 2000-2050 in the  
397 bottom panels of Figure 8. The GMI-DAS circulation has by far the greatest annual loss  
398 of  $\text{CFCl}_3$  and  $\text{CF}_2\text{Cl}_2$  (light blue dashed-dotted line in Figure 6) and the inferred fluxes are  
399 much greater than the expected zero value. For the three simulations with realistic age of  
400 air (CGCM, GMI-GCM and 2D-base) the simulated loss of  $\text{CFCl}_3$  is less than that  
401 required for consistency with the annual change in atmospheric burden, so the inferred  
402 fluxes are negative. Negative flux means that the  $\text{CFCl}_3$  is being removed from the  
403 atmosphere by processes other than the stratospheric losses, i.e., the mixing ratio  
404 boundary condition creates an artificial surface loss. For the CGCM simulations the  
405 negative flux of  $\text{CFCl}_3$  is about 20% of stratospheric loss after 2020. If we implemented  
406 flux boundary conditions in the CGCM, the burden of  $\text{CFCl}_3$  would decline more slowly  
407 than presently forecast.  
408  
409 The annual change in burden is generally better matched by the computed losses for  
410  $\text{CF}_2\text{Cl}_2$ . As for  $\text{CFCl}_3$ , GMI-DAS requires a significant positive flux to maintain  
411 consistency with the  $\text{CF}_2\text{Cl}_2$  burden. A small positive flux is calculated for 2D-fast. The

412 magnitudes of the inferred fluxes calculated for the CGCM (2 cases), GMI-GCM and 2D-  
413 base are within 5% of the annual loss.

414

415 We compare the lifetimes ( $\tau$  = model loss/model burden) that are internally calculated for  
416 the two CGCM simulations, GMI-GCM, 2D-base, GMI-DAS and 2D-fast in the top  
417 two panels of Figure 8. The  $\text{CFCl}_3$  lifetimes ~2005 are substantially longer than the 45  
418 year lifetime used in recent WMO assessments to produce the mixing ratio scenarios used  
419 by CGCM, GMI-GCM and 2D-base. The lifetime range for the models with realistic  
420 age-of-air, 56-64 years, is inconsistent with both the  $\text{CFCl}_3$  lifetime used in the WMO  
421 assessments and outside the observationally derived range of  $41 \pm 12$  years reported by  
422 *Volk et al.* [1997]; the quoted uncertainty of 12 years is one-sigma. The 2D-fast lifetime is  
423 the same value as used in assessments; the GMI-DAS lifetime is smaller but within the  
424 range derived by *Volk et al.* [1997]. The  $\text{CF}_2\text{Cl}_2$  lifetime for GMI-DAS (80 years) is close  
425 to the middle of the range derived by *Volk et al.* [1997], and is shorter than the lifetime  
426 used in assessments (100 years). The other simulations produce  $\text{CF}_2\text{Cl}_2$  lifetimes within  
427 10% of the lifetime used in the assessments.

428

429 The lifetimes in the CGCM simulations decrease with time throughout the integration  
430 because the overturning circulation speeds up, a common feature of this sort of model  
431 [*Butchart et al.*, 2006]. This will be discussed in Section 6.

432

433

434 **4. The relationship between mean age-of-air and fractional release**

435 In order to understand the relationship between the mean age-of-air and the fractional  
436 release (Figure 5), we have calculated age spectra using the 2D trajectory model  
437 following the approach of S2000. Five-year back trajectory histories are calculated for  
438 2000 parcels originally located within  $0.5^\circ$  latitude and 0.25 km of 55N, 21 km. This  
439 location is chosen to illustrate the relationships; other locations in the lower stratosphere  
440 extra-tropics behave similarly. To avoid confusion we refer to each parcel as an element  
441 of the age spectrum. The age spectrum produced by this calculation is shown in Figure  
442 9(a). The time when the each element crosses the tropical tropopause is its age – fewer  
443 than 1% of the 2000 parcels fail to cross the tropical tropopause during the integration.  
444 These elements are assigned an age of 5 years. The old age tail is obviously truncated by  
445 this approach, but resolving the tail would require thousands of elements and a much  
446 longer period of integration without impacting the results as will be clear from the  
447 discussion below.

448

449 The fractional releases of  $\text{CFCl}_3$  and  $\text{CF}_2\text{Cl}_2$  are calculated for each element using an  
450 annual mean loss rate. For each element an entry value for each CFC mixing ratio is  
451 calculated at the tropical tropopause using the time series of tropospheric mixing ratios  
452 and the age of the element. The amount of CFC remaining in each element is calculated  
453 by integrating forward from the tropical tropopause along the trajectories, interpolating  
454 the annual mean loss to the location of the element at each time step. The distributions of  
455 fractional release are given in Figure 9(b) for  $\text{CFCl}_3$  and 9(c) for  $\text{CF}_2\text{Cl}_2$ . The fraction of  
456 elements is shown on a log scale for  $\text{CFCl}_3$  and  $\text{CF}_2\text{Cl}_2$  to show that there are a few

457 elements that have lost most of their  $\text{CF}_2\text{Cl}_2$ . About 12% of the 2000 elements have lost  
458 more than 90% of their  $\text{CFCl}_3$ ; only 1% of the elements have lost a comparable fraction  
459 of  $\text{CF}_2\text{Cl}_2$ .

460

461 The relationship between the fractional release and the age spectrum is not obvious from  
462 the distributions shown in Figure 9. The relationship is clarified somewhat by plotting  
463 the fractional releases and the maximum altitudes experienced along the trajectories as  
464 functions of the age of the elements as shown in Figure 10.

465

466 For  $\text{CFCl}_3$  (Figure 10a) the relationship between the age of the element and fractional  
467 release is fairly compact and linear for ages less than 1.5 years; 35% of the elements fall  
468 in this range. For older ages a much wider range of fractional releases is possible; for  
469 ages greater than 3 years 10% of the elements have fractional releases of 0.95 or greater.

470 The maximum loss of  $\text{CF}_2\text{Cl}_2$  takes place at higher altitude (Figure 2), and this is  
471 reflected by Figure 10b. The relationship between fractional release and age is fairly  
472 compact and linear for element ages less than 2.5 – 3 years, but there is little correlation  
473 between the fractional release and element age for older ages. The relationship between  
474 the age of the element and the maximum altitude is also much more compact for elements  
475 younger than three years (Figure 10c). This result is consistent with the findings of *Hall*  
476 [2000] who also studied the maximum altitude distribution of elements of the age  
477 spectrum.

478

479 S2000 present a conceptual framework for the relationship between the mean age and the  
480 tracer amount for long-lived tracers and show that under an average path approximation

481 the tracer amount is more strongly related to the age than to the parcel path. The results  
482 of Figure 10 support the relationship between tracer amount and age for younger  
483 elements in the age spectrum but behavior is different for the older elements. We explore  
484 this result further by plotting the fractional release as a function of the maximum altitude  
485 experienced by the element (Figure 11). There is a compact relationship between the  
486 fractional release for each element and its maximum altitude for both CFCs. Elements  
487 with maximum altitudes greater than 30 km experience virtually complete loss of  $\text{CFCl}_3$   
488 and are insensitive to further increases in maximum altitude. For  $\text{CF}_2\text{Cl}_2$  the fractional  
489 release increases with increasing maximum altitude.

490

491 To clarify the relationship between the age of the elements and the maximum height, we  
492 bin the elements according to their ages (0-1 yr, 1-2 yr, etc.) and compute the mean and  
493 standard deviation of the age and the associated maximum heights. These are shown in  
494 Figure 12. Elements associated with older age intervals experience a much broader range  
495 of maximum heights than those with younger ones as was found by *Hall* [2000]. Also  
496 note that elements with ages younger than 3 years have fractional release values for  
497  $\text{CF}_2\text{Cl}_2$  less than 0.2 (Figure 10(b)), consistent with the result that the elements rarely if  
498 ever rise above 30 km and thus do not experience rapid destruction of  $\text{CF}_2\text{Cl}_2$ . This  
499 analysis shows that a significant fraction of the air in the lower stratosphere with mean  
500 age greater than a few years and fractional releases of  $\text{CF}_2\text{Cl}_2$  greater than 0.4 as reported  
501 by *Schauffler et al.* [2003] has at some time experienced heights above 30 km.

502

503 The simulated fractional release values for  $\text{CF}_2\text{Cl}_2$  and  $\text{CFCl}_3$  from the two simulations  
504 with fast circulations (GMI-DAS and 2D-fast) are greater for younger ages than those

505 calculated with the slower circulations. These values are also greater than observed.  
506 This result makes sense in the context of the trajectory calculations. The elements in the  
507 age spectra for the faster circulations must be associated with higher maximum altitudes  
508 than elements with similar ages from the age spectra for the slower circulations, thus  
509 more chlorine is released from the CFCs in these circulations even though their residence  
510 time in the stratosphere is reduced due to the more rapidly overturning circulation.

511

## 512 **5. Future age and fractional release distributions**

513 As noted above, the lifetimes of  $\text{CFCl}_3$  and  $\text{CF}_2\text{Cl}_2$  calculated for CGCM  
514 simulations decrease as the integrations progress (Figure 8). *Austin and Li* [2006] show  
515 that the mean age decreases as the strength of the overturning circulation increases using a  
516 similar CCM. The CGCM mean age decreases globally throughout the simulation; the  
517 difference in the zonal mean age between 1995 and 2045 is shown in Figure 13 for one  
518 simulation; all simulations show similar patterns. In the lower stratosphere the fractional  
519 release and mean age exhibit a compact relationship (Figure 5). The compact relationships  
520 change with time because the mean age is more sensitive to the simulated change in  
521 circulation than the fractional release (Figure 14). The mean age decreases everywhere in  
522 the stratosphere (Figure 13), but the fractional release can decrease, remain nearly  
523 constant, or can increase. We emphasize this point by computing the change in fractional  
524 release five year means centered on 2002 and 2047 in two ways. The changes for  $\text{CFCl}_3$   
525 and  $\text{CF}_2\text{Cl}_2$  are given in Figure 15(a) and 15(b). Figures 15(c) and 15(d) show the change  
526 for the same time period that would be obtained assuming a fixed relationship between

527 fractional release and mean age. Note that the changes are much larger for 15(c) and 15(d),  
528 and the scales also differ. Similar patterns are obtained for all simulations.  
529

530 As shown in Figure 13, the mean age is younger throughout the stratosphere; the largest  
531 changes are found at middle and high latitudes in the lower stratosphere. The patterns of  
532 change in fractional releases for  $\text{CFCl}_3$  and  $\text{CF}_2\text{Cl}_2$  are consistent with the change in the  
533 circulation. In the tropics parcels are transported upward more rapidly. Tracer profiles  
534 are displaced upward slightly leading to increased loss, but the fractional releases decrease  
535 due to a shorter residence time. The largest decrease in the fractional release of  $\text{CFCl}_3$  is  
536 seen in the region of maximum loss, i.e., between 50 and 30 hPa (Figure 2 and Figure 15a).  
537 For  $\text{CF}_2\text{Cl}_2$  the largest decrease in fractional release is between 20 and 5 hPa (Figure 2 and  
538 Figure 15b). Outside the tropics the fractional release changes very little as the mean age  
539 decreases, suggesting that although some elements in the age spectrum experience higher  
540 maximum heights and greater loss, this is balanced by the overall shift in the age spectrum  
541 towards younger ages. The shift in the relationship between the mean age and the  
542 fractional release as the circulation speeds up is explained by the relationships between  
543 the age spectrum, the maximum height, and the fractional release explored in the previous  
544 section. Figures 15c and 15d assume that the relationships between the fractional  
545 releases and the mean ages are unchanged, and show a completely different pattern from  
546 that produced by the CGCM simulations. Under this assumption, the fractional release  
547 would always decrease as the age decreases. The largest changes would occur in the

548 middle high latitude lower stratosphere, the opposite of what is produced by the  
549 simulations.

550

## 551 **6. Discussion and Conclusions**

552 In all current ozone assessment, ODS mixing ratios are specified as model boundary  
553 conditions. The use of these mixing ratio boundary conditions for the past record  
554 guarantees that the tropospheric mixing ratios match observations. Even so, the amount of  
555 inorganic chlorine in the atmosphere varies significantly among simulations because the  
556 loss rates of the chlorofluorocarbons vary for different circulations.

557

558 The modeled mixing ratios of  $\text{Cl}_y$  and HCl in the upper atmosphere are largely controlled  
559 by the mixing ratio boundary conditions; the exact timing of the maxima will vary if the  
560 times to propagate the boundary conditions to the upper atmosphere differ. The amount  
561 of  $\text{Cl}_y$  in the lower stratosphere is strongly influenced by differences in circulation among  
562 various simulations. If flux boundary conditions were used the level of  $\text{Cl}_y$  in the upper  
563 stratosphere and its rate of increase and decline would also vary depending on the  
564 simulation circulation and transport through their impact on the loss rate, and  
565 comparisons with time series would provide additional information about model  
566 performance. For example, *Lary et al.* [2007] have combined measurements of various  
567 chlorine species to produce a global estimate of  $\text{Cl}_y$  for 1991-2006. *Froidevaux et al.*  
568 [2006] demonstrate that upper stratospheric chlorine decreased between July 2004 and  
569 December 2005.

570

571 The question of the amount of chlorofluorocarbons that is presently ‘banked’ and the rate  
572 of release to the atmosphere is difficult to address. Top-down and bottom-up estimates  
573 differ, thus the projections for future atmospheric levels of CFCs are uncertain. We find  
574 that the magnitude of the fluxes needed to maintain the mixing ratio boundary conditions  
575 in our simulations depends on the overall vigor of the atmospheric circulation.  
576 Comparisons with observations presented by *Pawson et al.* [2007] as well as the  
577 comparisons with age-of-air and fractional release shown here indicate that the  
578 circulations and destruction rates of CGCM, GMI-GCM and 2D-base are more realistic  
579 than those of GMI-DAS and 2D-fast. An important implication of these results is that  
580 simulations with realistic age-of-air and fractional release of chlorine yield longer  
581 atmospheric lifetimes for chlorofluorocarbons. The effect is greater for  $\text{CFCl}_3$  (56 years  
582 vs 45 years) than for  $\text{CF}_2\text{Cl}_2$  (101-110 years vs 100 years). The difference in the loss  
583 estimates is comparable to the difference in the bank estimates for the ‘bottom up’ and  
584 ‘top down’ evaluations reported by *Daniel et al.* [2007]. If these longer lifetimes are  
585 more appropriate, the amounts of  $\text{CFCl}_3$  and  $\text{CF}_2\text{Cl}_2$  stored in banks estimated from  
586 bottom-up calculations would increase and agree better with the top-down estimates.  
587 Finally, we find that the lifetime decreases as the circulation speeds up due to climate  
588 change as in most CCM calculations. Flux boundary conditions for long-lived gases must  
589 be used to test whether the change in the loss due to the circulation speed-up has a  
590 significant impact on the decline of CFCs in the atmosphere.

591

592 **References**

- 593 Austin, J. and F. Li (2006), On the relationship between the strength of the Brewer-  
594 Dobson circulation and the age of stratospheric air, *Geophys. Res. Lett.*, *33*,  
595 doi:10.1029/2006GL026867.
- 596 Boering, K. A., S. C. Wofsy, B. C. Daube, H. R. Schneider, M. Loewenstein, and J. R.  
597 Podolske (1996), Stratospheric mean ages and transport rates from observations  
598 of carbon dioxide and nitrous oxide, *Science*, *274*(5291), 1340–1343.
- 599 Butchart, N., and A. A. Scaife (2001), Removal of chlorofluorocarbons by increased mass  
600 exchange between the stratosphere and troposphere in a changing climate, *Nature*,  
601 *410*, 799-802.
- 602 Butchart et al. (2006), Simulations of the anthropogenic change in the strength of the  
603 Brewer-Dobson circulation, *Clim. Dyn.*, *27*, 727-741.
- 604 Considine, D. B., A. R. Douglass, P. S. Connell, D. E. Kinnison, and D. A. Rotman,  
605 (2000), A polar stratospheric cloud parameterization for the global modeling  
606 initiative three-dimensional model and its response to stratospheric aircraft, *J.*  
607 *Geophys. Res.*, *105*, 3955-3973.
- 608 Daniel J. S., G. J. M. Velders, S. Solomon, M. McFarland, S. A. Montzka (2007), Present  
609 and future sources and emissions of halocarbons: Toward new constraints, *J.*  
610 *Geophys. Res.*, *112*, D02301, doi:10.1029/2006JD007275.
- 611 Douglass, A. R., C. H. Jackman, and R. S. Stolarski (1989), Comparison of model results  
612 transporting the odd nitrogen family with results transporting separate odd  
613 nitrogen species, *J. Geophys. Res.*, *94*, 9862-9872.

614 Douglass, A. R. and S. R. Kawa (1999), Contrast between 1992 and 1997 high-latitude  
615 spring Halogen Occultation Experiment observations of lower stratospheric HCl,  
616 *J. Geophys. Res.*, *104*, 18,739-18,754.

617 Douglass, A. R., M. R. Schoeberl, S. R. Kawa and E. V. Browell (2001), A composite  
618 view of ozone evolution in the 1995-1996 northern winter polar vortex developed  
619 from airborne lidar and satellite observations, *J. Geophys. Res.*, *106*, 9879-9895.

620 Douglass, A. R., M.R. Schoeberl, R. B. Rood and S. Pawson (2003), Evaluation of  
621 transport in the lower tropical stratosphere in a global chemistry and transport  
622 model, *J. Geophys. Res.*, *108*, 4259, 2002JD002696.

623 Douglass, A. R., R. S. Stolarski, S. E. Strahan, P. S. Connell (2004), Radicals and  
624 reservoirs in the GMI chemistry and transport model: Comparison to  
625 measurements, *J. Geophys. Res.*, *109*, D16302, doi:1029/2004JD004632.

626 Eyring V., et al. (2006), Assessment of temperature, trace species, and ozone in  
627 chemistry-climate model simulations of the recent past, *J. Geophys. Res.*, *111*,  
628 D22308, doi:10.1029/2006JD007327.

629 Feller, W., An Introduction to Probability Theory and Its Applications, vol. 1, John Wiley  
630 New York, 1968.

631 Fleming, E. L., C. H. Jackman, R. S. Stolarski, and D. B. Considine (1999), Simulation of  
632 stratospheric tracers using an improved empirically based two-dimensional model  
633 transport formulation, *J. Geophys. Res.*, *104*, 23911-23934.

634 Fleming, E. L., C. H. Jackman, D. B. Considine, and R. S. Stolarski (2001), Sensitivity of  
635 tracers and a stratospheric aircraft perturbation to two-dimensional model  
636 transport variations, *J. Geophys. Res.*, *106*, 14245-14263.

660 Kiehl, J.T., J.J. Hack, G.B. Bonan, B.A. Boville, D.L. Williamson, and P.J. Rasch (1998),  
661 "The National Center for Atmospheric Research Community Climate Model:  
662 CCM3" *J. Climate* 11, 1131-1149.

663 Lary D.J., D. W. Waugh, A. R. Douglass, R. S. Stolarski, P. A. Newman, H. Mussa  
664 (2007), Variations in stratospheric inorganic chlorine between 1991 and 2006,  
665 *Geophys. Res. Lett.* in press.

666 Lin, S.-J. and R. B. Rood, Multidimensional flux form semi-Lagrangian transport  
667 schemes, *Mon. Wea. Rev.*, 124, 2040-2070, 1996.

668 Lin, S.-J., A finite-volume integration scheme for computing pressure-gradient forces in  
669 general vertical coordinates, *Q. J. R. Meteorol. Soc.*, 123, 1749-1762, 1997.

670 Lin, S.-J. and R. B. Rood, An explicit flux-form semi-Lagrangian shallow water model on  
671 the sphere, *Q. J. R. Meteorol. Soc.*, 123, 2477-48, 1997.

672 Logan, J. A. (1999), An analysis of ozonesonde data for the troposphere:  
673 Recommendations for testing 3-D models and development of a gridded  
674 climatology for tropospheric ozone, *J. Geophys. Res.*, 104, 16,115-16,150.

675 McCulloch, A., P. Ashford, P. M. Midgley (2001), Historic emissions of  
676 fluortrichloromethane (CFC-111) based on a market survey, *Atmospheric*  
677 *Environment* 35, 4387-4397.

678 McCulloch, A., P. M. Midgley, P. Ashford (2003), Releases of refrigerant gases (CFC-  
679 12, HCFC-22 and HFC-134a) to the atmosphere, *Atmospheric Environment* 37,  
680 889-902.

637 Fleming, E. L., C. H. Jackman, D. K. Weisenstein, and M. K. W. Ko (2007), The impact  
638 of interannual variability on multi-decadal total ozone simulations, *J. Geophys.*  
639 *Res.*, *112*, D10310, doi:10.1029/2006JD007953.

640 Froidevaux L. et al. (2006), Temporal decrease in upper atmospheric chlorine, *Geophys.*  
641 *Res. Lett.*, *33*, L23812, doi:10.1029/2006HL027600.

642 Gupta, M. L., R. P. Turco, C. R. Mechoso and J. A. Spahr, On-line simulations of passive  
643 chemical tracers in the University of California, Los Angeles, atmospheric general  
644 circulation model 1. CFC-11 and CFC-12 (2001), *J. Geophys. Res.*, *106*, 12401-  
645 12417.

646 Hall, T. M. (2000), Path histories and timescales in stratospheric transport: Analysis of an  
647 idealized model, *J. Geophys. Res.*, *105*, 22811-22823.

648 Intergovernmental Panel on Climate Change/Technology and Economic Assessment  
649 Panel (2005), IPCC Special Report: Safeguarding the Ozone Layer and the Global  
650 Climate System: Issues Related to Hydrofluorocarbons and Perfluorocarbons, 478  
651 pp., Cambridge Univ. Press, New York.

652 Jackman, C. H., A. R. Douglass, R. B. Rood, R. D. McPeters, and P. E. Meade (1990),  
653 Effect of solar proton events on the middle atmosphere during the past two solar  
654 cycles as computed using a two-dimensional model, *J. Geophys. Res.*, *95*, 7417-  
655 7428.

656 Jacobson, M. Z. (1998), Improvement of SMVGEAR II on vector and scalar machines  
657 through absolute error tolerance control, *Atmos. Environ.*, *32*, 791-796.

658 Johns, T.C., et al. (2006), "The new Hadley Centre Climate Model (HadGEM1):  
659 Evaluation of coupled simulations", *J. Climate* *19*, 1327-1353.

681 Newman, P. A., E. R. Nash, S. R. Kawa, S. A. Montzka and S. M. Schauffler (2006),  
682 When will the Antarctic ozone hole recover, *Geophys. Res. Lett.*, 33, L12814,  
683 doi:10.1029/2005GL025232.

684 Pawson, S., R. S. Stolarski, A. R. Douglass, P. A. Newman, J. Nielsen, Mohan L.  
685 Gupta (2007), Goddard Earth Observing System chemistry-climate model  
686 simulations of stratospheric ozone-temperature coupling between 1950 and 2005,  
687 submitted to *J. Geophys. Res.*

688 Rayner, N. A., D. E. Parker, E. B. Horton, C. K. Folland, L. V. Alexander, D. P. Rowell,  
689 E. C. Kent and A. Kaplan, Global analyses of sea surface temperature, sea ice and  
690 night marine air temperature since the late nineteenth century (2003), *J. Geophys.*  
691 *Res.*, 108, 4407.

692 Sander, S. P., et al. (2003), Chemical kinetics and photochemical data for use in  
693 atmospheric studies, Evaluation number 14, JPL Publ. 02-25.

694 Schauffler, S. M., E. L. Atlas, S. G. Donnelly, A. Andrews, S. A. Montzka, J. W. Elkins,  
695 D. F. Hurst, P. A. Romashkin, G. S. Dutton and V. Stroud, Chlorine budget and  
696 partitioning during the Stratospheric Aerosol and Gas Experiment (SAGE) III  
697 Ozone Loss and Validation Experiment (SOLVE), *J. Geophys. Res.*, 108,  
698 doi:10.1029/2001JD002040, 2003.

699 Schoeberl, M. R., L. C. Sparling, C. H. Jackman, E. L. Fleming (2000), A Lagrangian  
700 view of stratospheric trace gas distributions, *J. Geophys. Res.*, 105, 1537-1552.

701 Stolarski, R. S., A. R. Douglass, M. Gupta, P. A. Newman, S. Pawson, M. R. Schoeberl  
702 and J. E. Nielsen (2006a), An ozone increase in the Antarctic summer

703 stratosphere: A dynamical response to the ozone hole, *Geophys. Res. Lett.*, 33,  
704 doi:10.1029/2006GLO26820.

705 Stolarski, R. S., A. R. Douglass, S. Steenrod, and S. Pawson (2006b), Trends in  
706 stratospheric ozone: Lessons learned from a 3D chemical transport model, *J.*  
707 *Atmos. Sci.*, 63, 1028-1041.

708 Strahan, S. E. and A. R. Douglass (2004), Evaluating the credibility of transport  
709 processes in simulations of ozone recovery using the Global Modeling Initiative  
710 three-dimensional model, *J. Geophys. Res.*, 109, D05110,  
711 doi:10.1029/2003JD004238.

712 Volk, C. M., J. W. Elkins, D. W. Fahey, G. S. Dutton, J. M. Gilligan, M. Loewenstein, J.  
713 R. Podolski, K. R. Chan, and M. R. Gunson (2003), Evaluation of source gas  
714 lifetimes from stratospheric observations, *J. Geophys. Res.*, 102, 25,543-25,564.

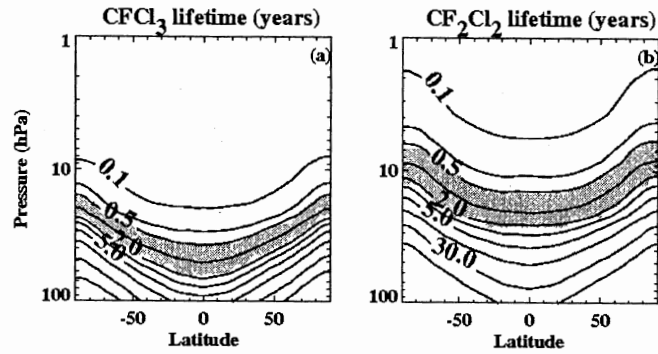
715 Waugh, D. W., S. E. Strahan, P. A. Newman (2007), Sensitivity of stratospheric  
716 inorganic chlorine to differences in transport, *Atmos. Chem. Phys.*, 7, 4935-4941.

717 World Meteorological Organization (WMO) (1985), *Atmospheric Ozone 1985:*  
718 *Assessment of our Understanding of the Processes Controlling its present*  
719 *Distribution and Change, Rep. 16*, Global Ozone Research and Monitoring  
720 Project, Geneva

721 World Meteorological Organization (WMO) (2003), *Scientific assessment of ozone*  
722 *depletion: 2002, Rep. 47*, Global Ozone Research and Monitoring Project,  
723 Geneva.

724 World Meteorological Organization (WMO) (2007), *Scientific assessment of ozone*  
725 *depletion: 2006, Rep. 50*, Global Ozone Research and Monitoring Project,  
726 Geneva.  
727  
728

729

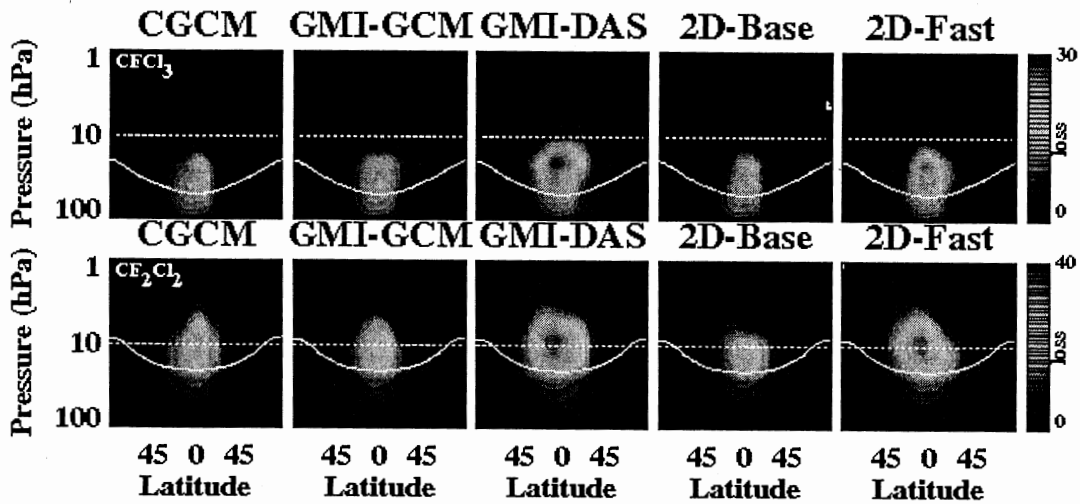


730

731 Figure 1 (a) Annual average local lifetimes as functions of latitude and altitude (pressure) for  
732  $\text{CFCl}_3$ ; (b) same as a for  $\text{CF}_2\text{Cl}_2$ .

733

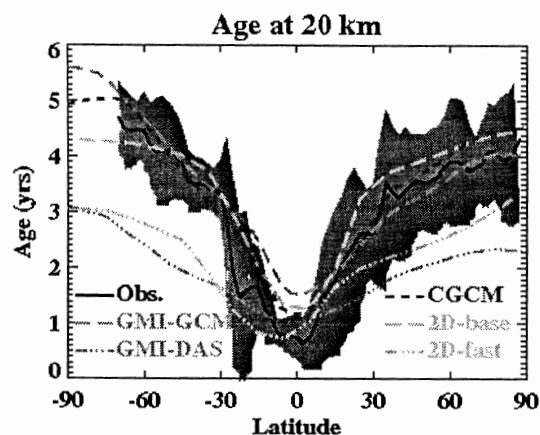
734



735

736 Figure 2 Loss rates ( $\#/ \text{cm}^3/\text{s}$ ) for  $\text{CFCl}_3$  (top row) and  $\text{CF}_2\text{Cl}_2$  (bottom row) as functions of  
737 latitude and altitude. Results are shown for five separate simulations indicated by the titles. The  
738 white dashed line is the 10 hPa level. The white solid line shows where the local lifetime is 1  
739 year. In the tropics the maximum loss is just above this threshold.

740

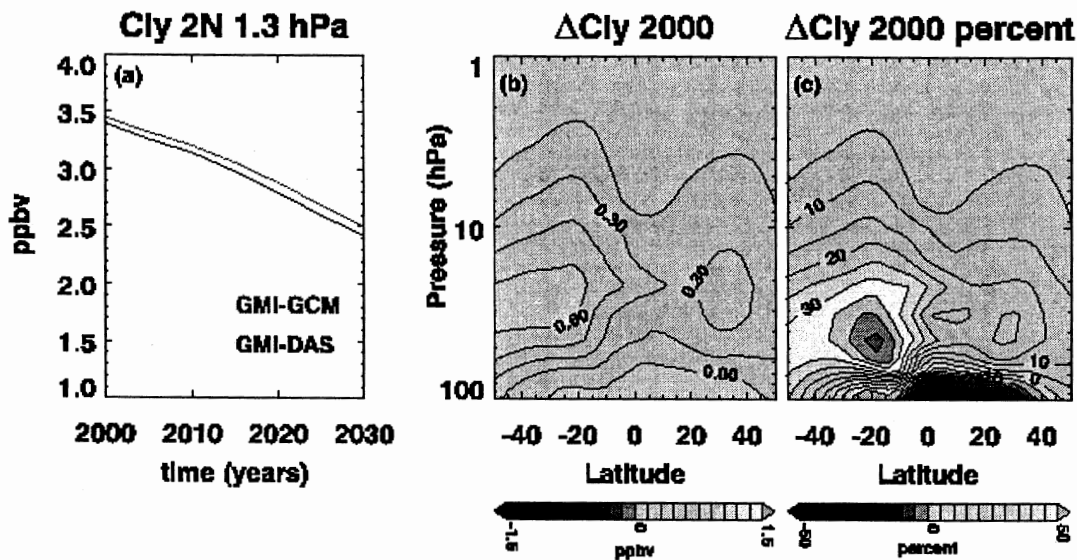


741

742 Figure 3: Age-of-air in the lower stratosphere from five simulations compared to data. The  
 743 CGCM, 2D-base and GMI-GCM produce a distribution for the age of air that is similar to that  
 744 observed; the GMI-DAS and 2D-fast ages are too young.

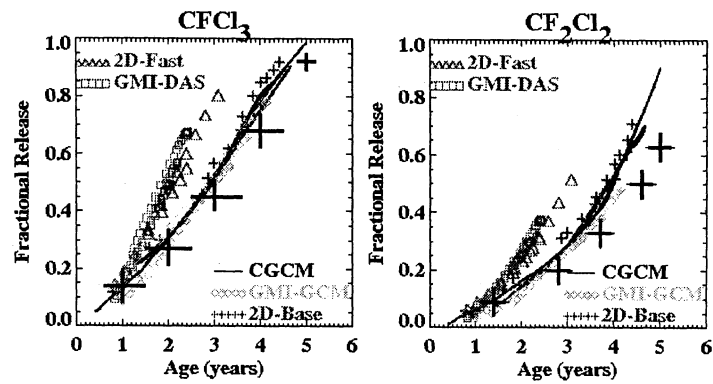
745

746



747

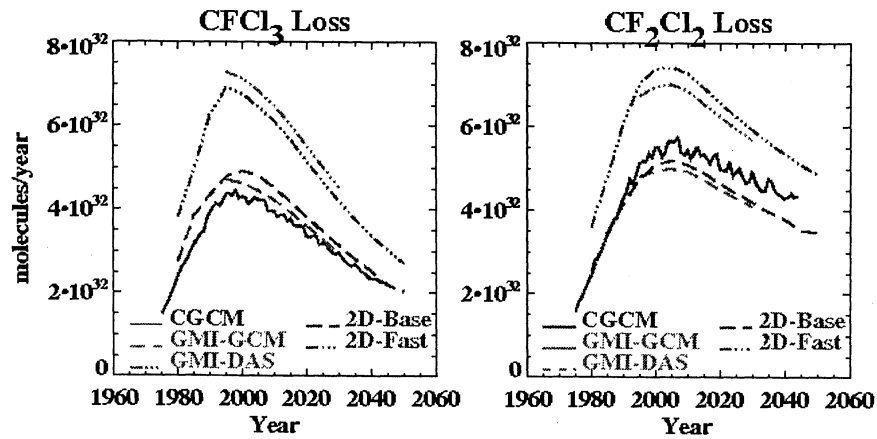
748 Figure 4(a) the  $Cl_y$  mixing ratios from GMI-GCM (blue) and GMI-DAS (black); (b) annual  
 749 average difference (ppbv)  $\Delta Cl_y = Cl_y^{GMI-GCM} - Cl_y^{GMI-DAS}$ ; (c) same as (b) in percent.



750

751 Figure 5 (a) The fractional release of  $CFCl_3$  relative to mean age from the simulations, northern  
 752 hemisphere 50-70 hPa, and the range of values from aircraft observations (large crosses) taken  
 753 from Figure 7 of *Schauffler et al.* [2003]; (b) same as (a) for  $CF_2Cl_2$ .

754

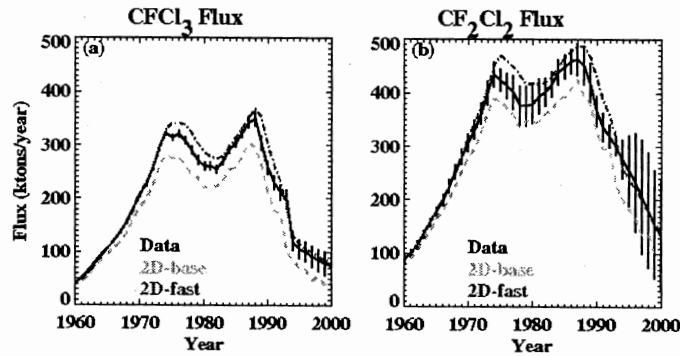


755

756 Figure 6 Annual-average loss for 1960 – 2060 for five simulations for (a)  $CFCl_3$  (b)  $CF_2Cl_2$ .

757

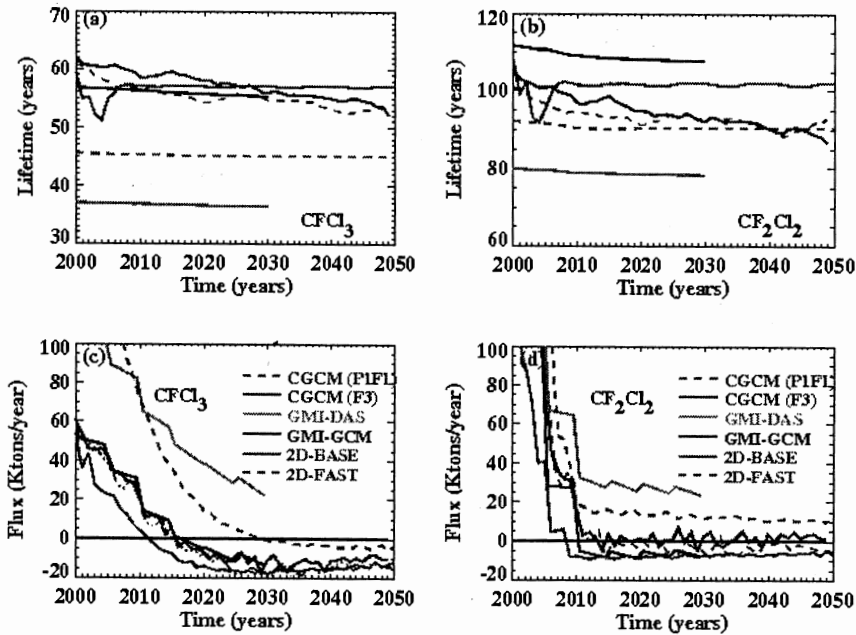
757



758

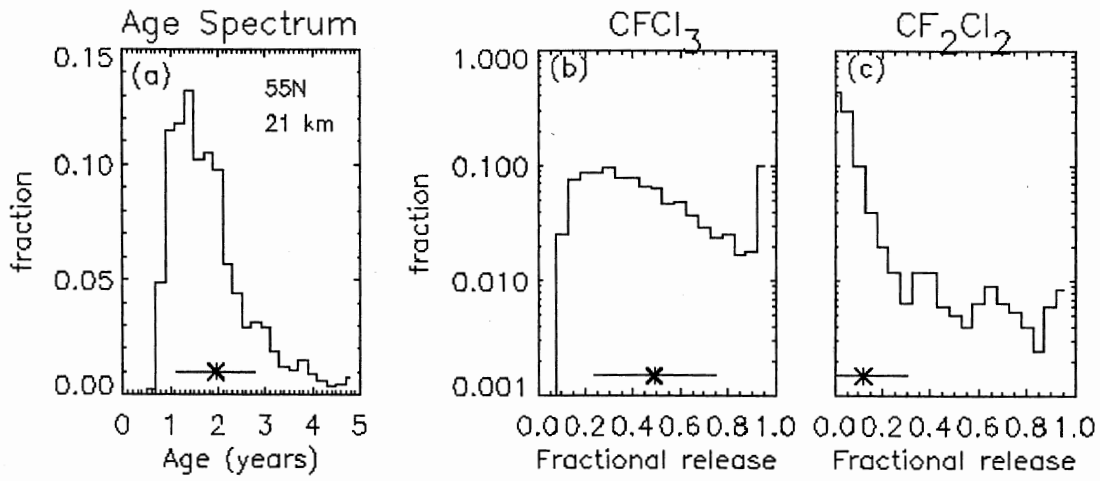
759 Figure 7(a) Computed fluxes of  $\text{CFCl}_3$  necessary to maintain the mixing ratio boundary  
760 conditions applied to the 2D-base and 2D-fast simulations. The  $\text{CFCl}_3$  data are the bottom up  
761 estimates of *McCullough et al.* [2001]; (b) same as (a) for  $\text{CF}_2\text{Cl}_2$ . The  $\text{CF}_2\text{Cl}_2$  data are taken  
762 from *McCullough et al.* [2003].

763



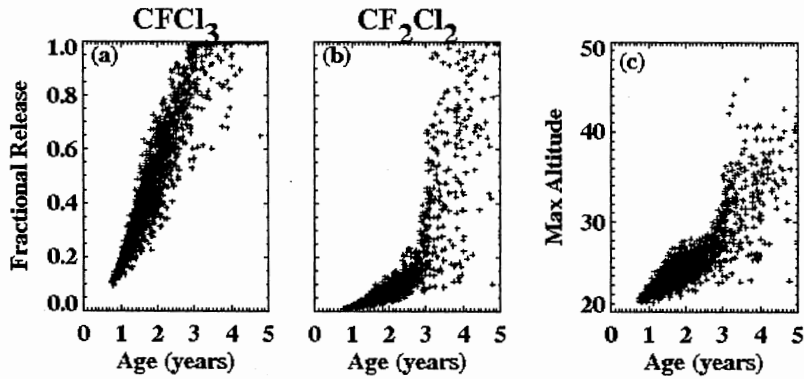
764

765 Figure 8(a) Lifetime of  $\text{CFCl}_3$  calculated internally from the five simulations; (b) same as (a) for  
766  $\text{CF}_2\text{Cl}_2$ ; (c) annual fluxes of  $\text{CFCl}_3$  implied by the annual change in the atmospheric burden and  
767 annual loss for the five simulations; (d) same as (c) for  $\text{CF}_2\text{Cl}_2$ .



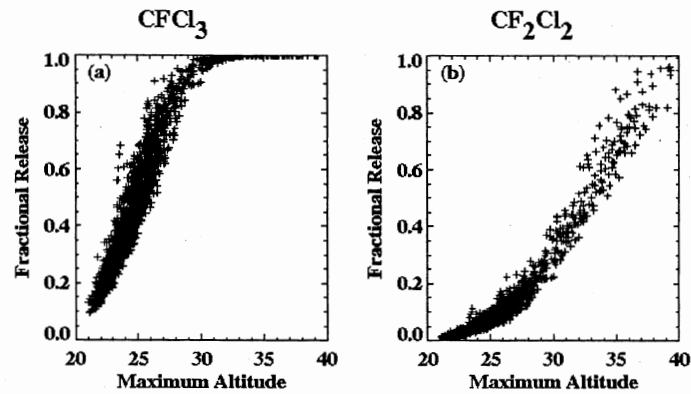
769 Figure 9(a) The age spectrum calculated using back trajectories from 55°N, 21 km; (b) the  
 770 distribution of fractional release values for CFC<sub>13</sub> calculated for the elements of the age  
 771 spectrum; (c) same as (b) for CFC<sub>2</sub>Cl<sub>2</sub>. On each panel the asterisk is the mean value and the  
 772 line is the standard deviation of the mean.  
 773

774



775  
 776  
 777 Figure 10 (a) The fractional release of CFC<sub>13</sub> computed using back trajectories for each  
 778 elements in the age spectrum; (b) same as (a) for CFC<sub>2</sub>Cl<sub>2</sub>; (c) the maximum altitude along the  
 779 trajectory for each element in the age spectrum.  
 780

780

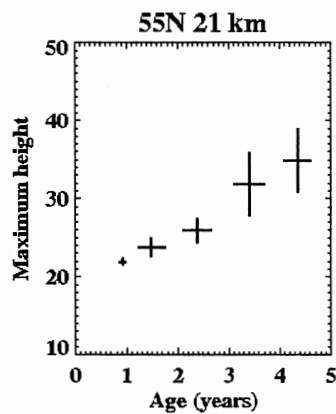


781

782

783 Figure 11 (a) The fractional release of  $\text{CFCl}_3$  as a function of the maximum altitude along  
784 the trajectory; (b) same as (a) for  $\text{CF}_2\text{Cl}_2$ .

785

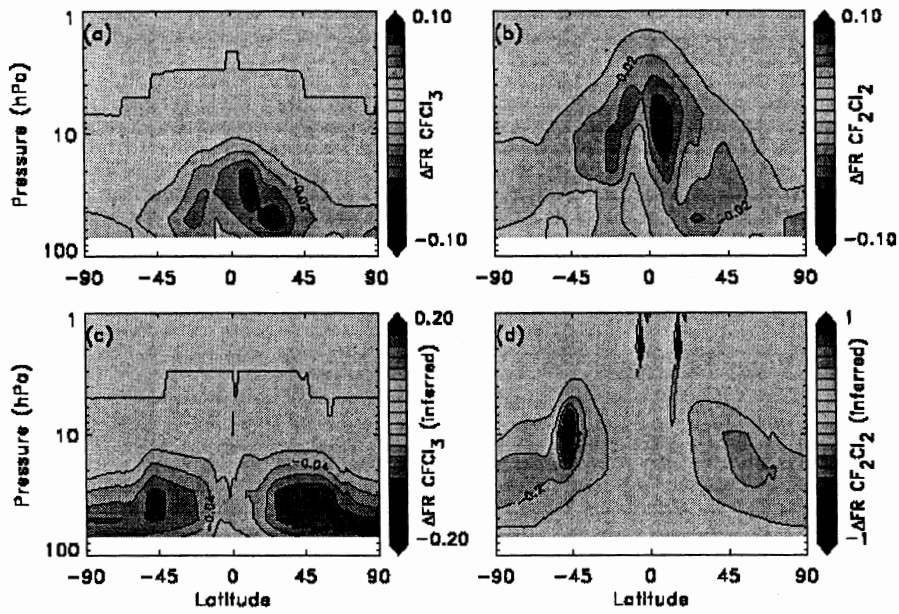


786

787 Figure 12 The mean maximum height and mean age for elements that are binned by age in single  
788 year intervals. The vertical and horizontal lines show the standard deviation of the maximum  
789 height and age respectively.

790

801

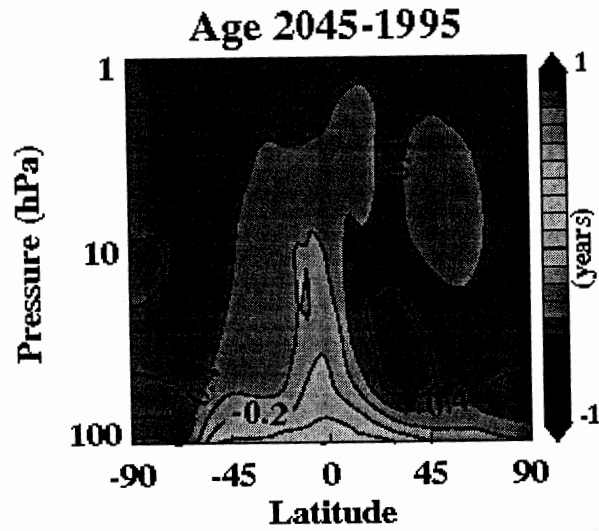


802

803 Figure 15(a) Changes in the fractional release distributions 2047 and 2002 for  $\text{CFC}_{13}$  as the  
804 circulation speeds up; (b) same as (a) for  $\text{CF}_2\text{Cl}_2$ . (c) Change in fractional release if the 2002  
805 relationship between  $\text{CFC}_{13}$  and mean age is unchanged; (d) same as (c) but for  $\text{CF}_2\text{Cl}_2$ .

806

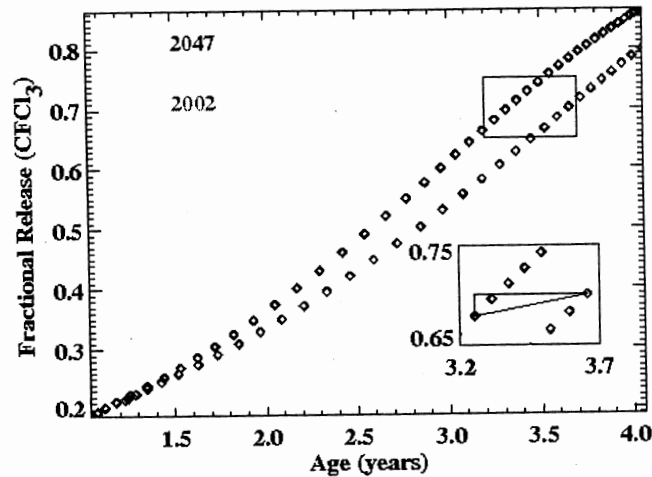
790



791

792 Figure 13: The annual average age-of air decreases throughout the stratosphere as shown by the  
793 difference between five-year averages centered on 2045 and 1995.

794



795

796 Figure 14: The relationship between mean age and fractional release changes as the residual  
797 circulation speeds up. The inset box magnifies the small unlabeled box to compare the change in  
798 age (x axis) with the change in fractional release (y axis) for 50°N, 50 hPa.

799

800